Theoretical framework for evaluation of x-ray spectra shape effects on dual-energy image quality

I. ROMADANOV[1], M. SATTARIVAND[1,2,3]

[1]Department of Medical Physics, Nova Scotia Health Authority, Halifax, NS,Canada.

[2]Department of Physics & Atmospheric Science, Dalhousie University, Halifax, NS,Canada.

3Department of Radiation Oncology, Dalhousie University, Halifax, NS, Canada.

JULY 12–16 2020 VIRTUAL JOINT AAPM | COMP MEETING

Improving Health QUALITY, Increasing Global IMPACT

EASTERN TIME [GMT-4]

INTRODUCTION

Dual-energy (DE) x-ray imaging relies on the difference in dominant attenuation mechanisms for spectra with different effective energies: lower energy photons are predominantly attenuated due to the photo-electric mechanism, and higher energy photons are Compton scattered. This can be exploited by acquiring two images with different x-ray spectra and then extracting material-specific information. Energy separation (ratio of spectra average energies) is commonly used to optimize x-ray spectra [1,2]. Spectra shapes were shown to play a significant role in the image quality as well [3-5].

AIM

This study is devoted to the development of a theoretical framework which allows for the investigation of the effects of x-ray spectra shape, incident on the object, on the resulting dual-energy (DE) image quality. Here, the image quality was quantified in terms of the contrast-to-noise ratio (CNR). Spectrum shape is described in terms of the physical parameters, such as spectrum average energy E^{avg}, x-ray tube potential E^{max} (kVp), and total photon fluence α (mAs). Thus, this description assists in gaining a better understanding of the effects of these parameters on the image quality.

METHOD

Spectra shape incident on the object is described with a fitting function, which resembles physical processes occurring during x-ray generation: bremsstrahlung radiation and its attenuation in the anode and follow up filtration [5]. A virtual phantom was used to evaluate CNR.

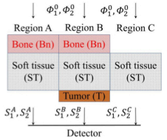

Figure 1. Virtual phantom to calculate CNR. $\Phi_{1,2}^0$ are initial spectra of HE, LE beams with. $S_{1,2}^{A,B,C}$ are the resulting signals as incident on the detector for regions A, B, and C respectively. Bn = 3 cm, ST = 30cm,T = 2 cm.

The CNR expression was derived as a function of spectra parameters and was parametrically analyzed. The optimal spectra parameters for a given set of kVp were found by optimizing the CNR expression. Optimization was performed with Matlab *fmincon* function. Simulations were conducted for two cases: without any limitations on input parameters, and with applied limitations on patient surface dose (ESD), which was calculated with AAPM TG61 protocol.

THEORY

Spectrum shape was approximated with the Rigaud spectrum [5]

$$\Phi(E) = \alpha\left(\frac{E^{max}}{E} - 1\right)e^{-\frac{\beta}{E^3}}, (1)$$

where α is the total photon fluence, E^{max} is the maximum spectrum energy, and β is the fitting parameter, representing attenuation in the target and follow-up filtration. Examples of this function and fitting of Spektr3.0 generated spectrum, which was done by matching practical physical parameters, are shown in Fig. 2.

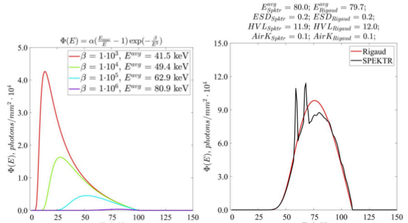

Figure 2. Fitting function (Eq. 1) for several values of β at fixed α. Fitting with Eq. 1 for 110 kVp spectrum.

Detector signal S_i and noise σ_i were related to the input spectrum as

$$S_i = \alpha_i \int_0^{E_i^{max}} \Phi_i(E)T(E)EdE\,;$$

$$\sigma_i^2 = \alpha_i \int_0^{E_i^{max}} \Phi_i(E)T(E)E^2dE\,,$$

where $T(E)$ is the transmittance function, described by Beer's law, which is object dependent. The CNR of soft-tissue DE for the virtual phantom in Fig. 1 is derived as

$$CNR = \frac{\frac{S_1^A}{(S_2^A)\omega} - \frac{S_1^B}{(S_2^B)\omega}}{\sqrt{\left(\frac{S_1^A}{(S_2^A)\omega}\right)^2\left[\left(\frac{\sigma_1^A}{S_1^A}\right)^2 + \omega^2\left(\frac{\sigma_2^A}{S_2^A}\right)^2\right] + \left(\frac{S_1^B}{(S_2^B)\omega}\right)^2\left[\left(\frac{\sigma_1^B}{S_1^B}\right)^2 + \omega^2\left(\frac{\sigma_2^B}{S_2^B}\right)^2\right]}}. (2)$$

After some manipulations this can be written as

$$CNR = \frac{1}{\sqrt{3}}\frac{\frac{T_1^A}{(T_2^A)\omega} - \frac{T_1^B}{(T_2^B)\omega}}{\sqrt{\left(\frac{T_1^A}{(T_2^A)\omega}\right)^2\left[\frac{1}{T_1^A}\frac{1}{\alpha_1}\frac{E_1^{avg}}{(E_1^{max})^2}\frac{1}{f_s(\beta_1')} + \omega^2\frac{1}{T_2^A}\frac{1}{\alpha_2}\frac{E_2^{avg}}{(E_2^{max})^2}\frac{1}{f_s(\beta_2')}\right] + \left(\frac{T_1^B}{(T_2^B)\omega}\right)^2\left[\frac{1}{T_1^B}\frac{1}{\alpha_1}\frac{E_1^{avg}}{(E_1^{max})^2}\frac{1}{f_s(\beta_1')} + \omega^2\frac{1}{T_2^B}\frac{1}{\alpha_2}\frac{E_2^{avg}}{(E_2^{max})^2}\frac{1}{f_s(\beta_2')}\right]}}. (3)$$

In this expression, $\beta_i' = \beta/(E_i^{max})^3$, and $f_s(\beta_i')$ is some function of β_i' after the integration. By using this expression, one can investigate the effects of individual spectrum parameters (α, E^{max}, E^{avg}) on the image CNR.

RESULTS

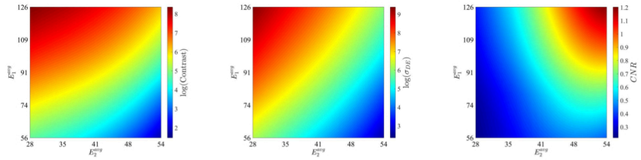

Figure 3. Effect of average beam energies on DE contrast (*left*) noise (*middle*), and CNR (*right*) for regions A and B of phantom in Fig. 1. E_i^{avg} is $\sim f(\beta_i')$. α_i were varied in a way that $\alpha_1\int_0^{E_1^{max}}\Phi_1(E)dE = \alpha_2\int_0^{E_2^{max}}\Phi_2(E)dE$

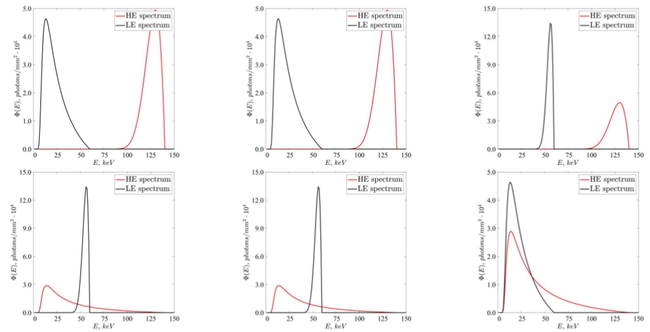

Figure 4. *Top row (from left to right):* spectra corresponding to maximum of DE contrast, noise, and CNR.
Bottom row (from left to right): spectra corresponding to minimum of DE contrast, noise, and CNR.

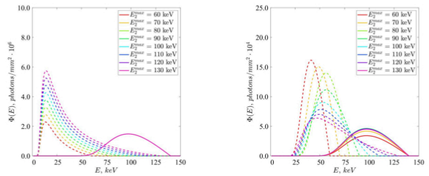

Figure 5. Optimized spectra to achieve max DE CNR for different combinations of high and low energy tube potentials (E^{max}). *Left:* no dose limitations. *Right:* with applied dose limitations. The corresponding CNRs are in Fig. 6.

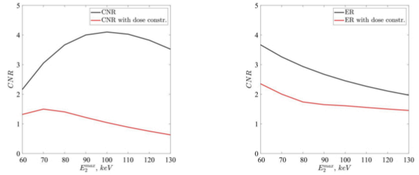

Figure 6. CNR (*Left*) and energy ratio, E_1^{avg}/E_2^{avg} (*Right*) for spectra shown in Fig. 5. *Black* – no dose limitations. *Red* – with dose limitations.

DISCUSSION AND CONCLUSIONS

A theoretical model describing the spectral shape effects on the resulting DE CNR was developed and investigated. Parametric investigation of Eq. 3 demonstrated that spectra separation (E_1^{avg}/E_2^{avg}) affects DE contrast and noise differently. Contrast is maximized for the largest spectra separation, but the opposite is true for noise. This is because the contrast is defined by the difference in average attenuation coefficients ($\mu^{avg}\sim E^{avg}$), while noise is dependent on signal levels. Noise is lower for stronger signals, what, in the case of fixed tube current, it corresponds with a wider spectrum [6]. Another way to reduce noise is by increasing the total fluence (α, see Eq. 3). The maximum of the CNR occurs for the intermediate case (see Fig. 4).

Optimization for a combination of different E^{max} was conducted in two cases: with and without dose limitations. The highest CNR without dose limitations (Fig. 5 left) is achieved when the energy ratio is far from maximum, showing the importance of the noise component. However, this is not a clinically relevant case, and the results with dose limitations (Fig. 5, right) have more practical meaning. Dose limitations force the optimization algorithm to select spectra with a minimized low-energy component, which makes them narrower. In this case, the contrast part has a stronger effect on the resulting CNR, and the peak occurs when the energy ratio is close to the maximum.

To summarize, optimal spectra for the maximized CNR of the DE image should provide not only maximized energy separation, but minimized noise. These two requirements contradict each other, even for the realistic case of dose limitations. This can be overcome by narrowing high and low energy spectra and increasing photon fluence (approaching monoenergetic spectra), or by maximizing the spectrum width, while keeping spectra separation maximized.

ACKNOWLEDGEMENTS

This work was supported by the ACOA (Atlantic Canada Opportunities Agency) Atlantic Innovation Fund.

REFERENCES

1. Primak, A.N., Ramirez Giraldo, J.C., Liu, X., Yu, L. and McCollough, C.H., Improved dual-energy material discrimination for dual-source CT by means of additional spectral filtration. Med. Phys., 36, 1359-1369, 2009.
2. Glick SJ, Thacker S, Gong X, and Liu B, Evaluating the impact of x-ray spectral shape on image quality in flat-panel CT breast imaging. Medical Physics, 34(1), 5–24,2007.
3. Makeev AV, Glick SJ. Investigation of x-ray spectra for iodinated contrast-enhanced dedicated breast CT. Journal of Medical Imaging, 4(1), 1 – 10, 2017.
4. Wong J, Xu T, Husain A, Le H, and Molloi S, Effect of area x-ray beam equalization on image quality and dose in digital mammography. Physics in Medicine and Biology, 49(16), 3539–3557, 2004.
5. Ho J-T, Kruger RA, and Sorenson JA, Comparison of dual and single exposure techniques in dual-energy chest radiography. Medical Physics, 16(2), 202–208, 1989.
6. Rigaud G, On analytical solutions to beam-hardening. Sensing and Imaging, 18(1), 5, 2017.
7. Alvarez RE, Dimensionality and noise in energy selective x-ray imaging. Medical physics 40(11), 111909, 2013.

CONTACT INFORMATION

Ivan.Romadanov@nshealth.ca, Mike.Sattarivand@nshealth.ca